

**Single Crystal Fluorescence Behavior of a New HOF Material:
Potential Candidate for a New LED**

Journal:	<i>Journal of Materials Chemistry C</i>
Manuscript ID	TC-ART-04-2018-001808.R1
Article Type:	Paper
Date Submitted by the Author:	18-May-2018
Complete List of Authors:	Gomez Garcia, Eduardo; Facultad de Ciencias del Medio Ambiente, Quimica Fisica Gutiérrez Tovar, Mario; Facultad de Ciencias Ambientales y Bioquimicas and INAMOL, UCLM, Quimica Fisica Toledo, Spain, Physical Chemistry Cohen, Boiko; Universidad de Castilla-La Mancha, Facultad de Ciencias del Medio Ambiente, Dept de Quimica Fisica Hisaki, Ichiro; Osaka University, Department of Material and Life Science Douhal, Abderrazzak; Facultad de Ciencias del Medio Ambiente, Dept de Quimica Fisica

Single Crystal Fluorescence Behavior of a New HOF Material: Potential Candidate for a New LED

Eduardo Gomez,[†] Mario Gutiérrez,[†] Boiko Cohen,[†] Ichiro Hisaki,^{§*} and
Abderrazzak Douhal^{†*}

[†]Departamento de Química Física, Facultad de Ciencias Ambientales y Bioquímica, and
INAMOL, Universidad de Castilla-La Mancha, Avenida Carlos III, S.N., 45071 Toledo, Spain.

[§] Department of Material and Life Science, Graduate School of Engineering, Osaka University,
2-1 Yamadaoka, Suita, Osaka 565-0871, Japan.

*Corresponding author: E-mail address: abderrazzak.douhal@uclm.es

E-mail address: hisaki@mls.eng.osaka-u.ac.jp

Abstract

Hydrogen-bonded Organic Frameworks (HOFs) have emerged as exciting new materials, due to several promising applications in science and technology. Using fluorescence microscopy, we report on spectral and dynamical characterization of a HOF (T12-apo), its parent compound (T12) and its ester-methylated derivative (T12-Ester) in solid state. In contrast to the behavior in solution, the absorption spectra of these solid materials exhibit a strong $S_0 \rightarrow S_1$ transition. The fluorescence microscopy studies of crystals of T12 reveal no crystal size effect on the emission spectra and lifetime (~38 ns). While, those of T12-Ester exhibit a photodynamic behavior that depends on their sizes. The large crystals exhibit a monoexponential behavior (~28 ns), while the smaller ones present an additional shorter component (~5 ns) due to the relaxation of species having a charge-transfer character. For T12-apo, the results suggest two types of crystals: i) those formed by π - π stacking, showing a photobehaviour similar to those of T12 and T12-Ester, and ii) crystals, in which the H-bonds between the building blocks play an important role, and result in different emission spectra and shorter fluorescence lifetimes compared to the formers. Moreover, the anisotropy measurements of large T12-apo crystals confirm the importance of π - π stacking of the aromatic core and of H-bonding interactions to form the HOF, and their relevance to the photobehaviour. We suggest to use the HOF to build a White-LED, when combined with a blue-light emitting LED. Our results provide new information on the photobehaviour of this HOF at single crystal level looking for its use in optoelectronic devices.

Keywords: Dehydrobenzoannulene derivatives, HOFs, Solid State, Luminescent, Single crystal microscopy, Time-resolved photodynamics.

1. Introduction

During the last two decades, porous materials have attracted the attention of the scientific community due to the broad range of their applications.¹⁻³ Among these materials, Metal Organic Frameworks (MOFs)⁴ and Covalent Organic Frameworks (COFs)⁵⁻⁶ have emerged as the most studied ones owing to their wide applicability in different fields of science and technology, such as selective gas sorption and storage, chemical luminescent sensors, catalysis and optoelectronics to cite some of them.⁷⁻²⁰

Recently, a new family of materials called Hydrogen-Bonded Organic Frameworks (HOFs) have been reported as an exciting new class of materials constructed solely using organic molecules connected by non-covalent H-bonding and π - π interactions.²¹ By a rational design and selection of the organic building blocks, the control of the crystalline structure as well as their pore size become possible. This advance allows the tunability of their physicochemical properties, making them versatile for different applications, such as gases storage and separation, proton conduction, and explosive detection.²²⁻²⁶ For example, a recent report has demonstrated how the luminescent HOF-1111 (composed by the fluorescent linker tetraphenylethylene) is able to detect several aromatic compounds, including nitroaromatic explosive like molecules.²⁵ Few years ago, taking advantage of the planarity and high π -conjugation of the dehydrobenzoannulenes (DBAs), these are being used as building blocks to synthesize new HOFs.^{24, 27-30} The molecular structure of the DBA units are paramount for the morphology, crystallinity and pore size of the HOFs, where π - π and H-bond interactions play a great role.³¹

Since their discovery, most of the research efforts has been focused on their synthesis and control of their porosity.^{21, 23, 32-33} However, their photophysical and photochemical properties remain largely unexplored. To the best of our knowledge, only

few studies have reported on the emission behavior (steady-state) of few HOFs.^{25, 34-35} Recently, we have reported on the time-resolved photobehaviour of CPHAT (carboxylphenyl substituent hexaazatriphenylene) HOF.³⁵ We demonstrated that the fundamental unit of the HOF in solution (*N,N*-dimethylformamide, DMF) undergoes an ultrafast intramolecular charge-transfer reaction followed by an intermolecular proton-transfer event with the DMF molecules, giving rise to a largely Stokes shifted emission band. Moreover, experiments using fluorescence microscopy on single crystals of the HOF (CPHAT-1a) showed a well ordered crystalline structure with preferential orientation of the molecular dipole moments.

We have also reported on the solution photobehaviour of the organic blocks of the crystals studied in the present work: Nu-T12 (5,6,11,12,17,18-hexadehydrotribenzo[a,e,i]cyclododecene), T12-COOMe (5,6,11,12,17,18-hexadehydro-2,3,8,9,14,15-hexakis(4-methoxycarbonylphenyl)tribenzo[a,e,i]cyclododecene) and T12-COOH (5,6,11,12,17,18-hexadehydro-2,3,8,9,14,15-hexakis(4-carboxyphenyl)tribenzo[a,e,i]cyclododecene).³⁶ We found that the $S_0 \rightarrow S_1$ transition of these molecules in solution is forbidden, in agreement with the theoretical calculations. Time-resolved experiments have revealed emission decays from locally excited state, charge-transfer and triplet states of Nu-T12 and T12-COOMe molecules. On the contrary, the behavior of T12-COOH ones strongly depends on the medium. For example, T12-COOH in a DMF solution forms new species having a long fluorescence lifetime (~26 ns) and large-shifted emission band; while in dimethylsulfoxide it exhibits similar photodynamical behavior to that of Nu-T12 and T12-COOMe. Aiming the exploration of the photobehaviour of materials based on these molecules, we performed a detailed

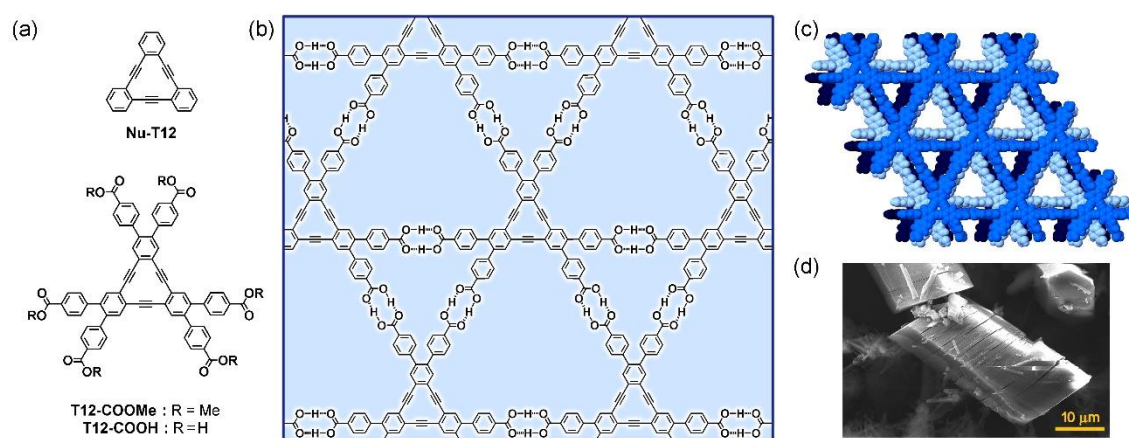
photophysical study of them. Such knowledge will help in designing and optimizing new HOFs for applications in OLEDs.

Here, we report on spectroscopic study of a HOF based on a DBA derivative (T12-apo) and its related materials, T12 and T12-Ester in the solid state (Scheme 1). Fluorescence lifetime imaging (FLIM) experiments of T12, T12-Ester, and T12-apo show homogeneous lifetime distribution. For T12, the emission spectra and lifetime do not depend on the crystal size, which are formed as a result of π - π stacking interactions. For T12-Ester, we found a difference in the photobehaviour between the large and small crystals, where an additional short component is observed in the case of the smallest one. The corresponding lifetime is attributed to the excited charge transfer species. The HOF of T12-apo exhibits emission and photodynamic behavior that depend on the crystal nature. On one hand, there is a family of crystals, whose photobehaviour is comparable to that observed for T12 and T12-Ester. On the other hand, another class exhibits a different photobehaviour suggesting that the H-bond interactions play an important role in the morphology of these crystals. The anisotropy behavior of the HOF, T12-apo indicates that the molecular units adopt preferential orientation inside the crystals. Our results give new insight for better understanding the photobehaviour properties of HOF that can be the basis for new optoelectronic devices. Our preliminary results suggest further studies to improve the HOF building blocks for lighting (OLEDs).

2. Experimental Section

The molecular blocks, Nu-T12, T12-COOME and T12-COOH (Scheme 1) were synthesized following the process described elsewhere.³⁷⁻³⁸ Briefly, Nu-T12 was synthesized via palladium-copper catalysed cyclization under phase transfer conditions. T12-COOME was synthesized by Castro-Stephens cyclization reaction and finally T12-COOH was then obtained by hydrolysis of T12-COOME. Solid materials of T12 and T12-

Ester were prepared by slow evaporation of chloroform solutions of Nu-T12 and T12-COOMe, respectively. HOF T12-apo was prepared by soaking of the as-formed crystalline powder, which was obtained by recrystallization of T12-COOH from a mixed solution of DMF and 1,2,4-trichlorobenzene, into benzene for overnight at room temperature, followed by lying under vacuum (0.2 kPa) for 1 day at 50 °C. The morphology of the solid materials was obtained by using a JEOL Ltd model JSM-7001F scanning electron microscope (SEM).



Scheme 1. (a) Molecular structures of Nu-T12, T12-COOMe and T12-COOH that constitute the units of the studied materials. (b) Illustration of the H-bond interactions between the molecular units of T12-apo HOF. (c) Top view of three layer packing of T12-apo. (d) SEM image of T12-apo.

The steady-state Infrared (IR) and UV-visible absorption spectra have been recorded using FT/TR-4200 (JASCO Inc.) and JASCO V-670 spectrophotometers, respectively. The fluorescence lifetime imaging (FLIM) measurements were performed on a MicroTime 200 confocal microscope (PicoQuant). As an excitation source, we used a diode laser with an excitation wavelength of 390 nm (40 ps full width at half-maximum of intensity). Briefly, it consists of inverse Olympus IX 71 microscope equipped with a water immersion objective (x60 NA1.2, Olympus) and 2D piezo scanner (Physik

Instrumente). The emitted light is then focused on a pinhole of 50 μm and later collimated to two independent single photon avalanche photodiodes (Micro-Photon-Devices) for time-resolved measurements. The emission spectra were collected through Shamrock SR-303i (Andor Technology) imaging spectrograph and detected by Andor Newton EMCCD camera (Andor Technology). For the anisotropy measurements the light was passed through a polarizing beam-splitter that allows for the simultaneous detection of the parallel and perpendicular parts of the emission. A G-factor of 1.2, accounting for differences in the detection sensitivity for both polarizations in the setup, was used in the calculation of the anisotropy. Moreover, to calculate the histogram of anisotropy, we used SymPhoTime Analysis program (which is facilitated by PicoQuant), which calculates the static anisotropy on an image. The analysis is based on the work of Schaffer group.³⁹ The limits for the anisotropy are -0.5 to 1.0, in which -0.5 correspond to perpendicular orientation and 1.0 to parallel. For each sample between 8 and 15 crystals have been analysed both in spectral and kinetic modes. The emission signal was collected using two long pass filters (HQ430LP and HQ530LP Chroma) and a band filter: FF01-503/40, Chroma. Finally, CIE coordinates of T12-apo were calculated using GoCIE software. The emission spectrum of T12-apo in solid state at room temperature was used to get the CIE coordinates.

3. Results and Discussion

3.1. Steady-State IR and UV-visible Absorption Studies

To begin with, we recorded the IR spectra of T12, T12-ester and T12-apo in solid state (Figures 1a and S1a). T12 displays two main peaks at 1486 and 750 cm^{-1} assigned to the C-C stretching of the benzene rings, and to the C-H out-of-plane bending, respectively. The peak at 750 cm^{-1} is present as a doublet, which suggests difference in the C-H out-of-plane bending modes related to the hydrogen atoms in the benzene ring.

The IR spectra of T12-ester and T12-apo are very rich and reflect the presence of the ester and carboxylic groups. The intense peak at 1100 cm^{-1} corresponds to the stretching of the methyl ester and thus it is observed only for T12-ester. The C=O stretching (1715 cm^{-1}) and the O-C bending (1435 cm^{-1}) for T12-ester shift to 1685 and 1419 cm^{-1} , respectively, for T12-apo. This shift is concomitant with an increase in the width of the peaks that also become less intense. The observed change reflects an explained by increased conjugation along with a strong H-bonding interaction in the T12-apo solid. Additionally, both T12-ester and T12-apo display two well separated peaks at 775 and 705 cm^{-1} with equal intensity instead of the doublet observed for T12 at 750 cm^{-1} . This change can be explained in terms of the presence of two different C-H out of plane bending modes in T12-ester and T12-apo, the C-H bond of the benzene rings in the core structures, and the C-H bonds in the benzene rings of the surrounding groups. We also examined the IR spectrum of the T12-apo at higher wavenumbers (Figure S1a). We observed only a weak and broad absorption peak at $\sim 3100\text{ cm}^{-1}$, assigned to the presence of O-H of the acid groups. The lack of strong O-H signal suggests strong H-bonding interactions of the units in T12-apo that reduce the intensity of OH vibrations.

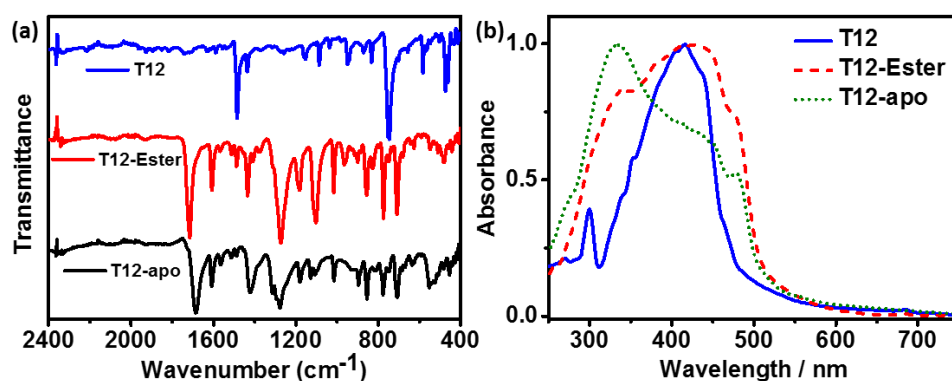


Figure 1. (a) Infrared absorption spectra of T12, T12-ester and T12-apo in solid state. (b) UV-visible absorption spectra of T12, T12-Ester and T12-apo (black dotted line) in solid state.

To better characterize the T12-apo based HOF, we collected the SEM images (Scheme 1B and Figure S1b-S1c). These show the formation of small and large well-ordered crystals and the presence of small fissures parallel to the crystal layer. These fissures were generated during the activation (desolvation) of the as-formed crystals of T12-apo. As previously reported,³⁷ some solvent molecules can be incrustated in the void space of T12-COOH crystals and when are removed, by heating the material under vacuum condition, an inter-layer slippage between the H-bonded network sheets occur. The inset of Scheme 1B shows a crystal structure of T12-apo determined by Rietveld refinement of powder X-ray diffraction pattern of the activated crystalline bulk of T12-COOH. The structure is composed of stacked layers of H-bonded, hexagonally-networked sheets and quasi-orthogonally running one-dimensional channels with triangular cross section. The fissures observed on the crystal in SEM images correspond to those between the molecular layers caused by interlayer dissociation.

The aim of this report is to characterize the photodynamic of these materials. Hence, we first collected the steady-state UV-visible absorption of T12, T12-Ester and T12-apo in solid state (Figure 1b). The absorption spectra of these materials consist of a broad band with the intensity maximum located at 416 nm for T12, 433 nm for T12-Ester, and 330 nm for T12-apo. However, the spectra of T12-ester and T12-apo present one more peak at 475 and 480 nm, respectively. These peaks correspond to 0-0 transition for $S_0 \rightarrow S_1$. T12 does not show such peak, but a clear and well-defined band is recorded at 299 nm, which is most probably related to $S_0 \rightarrow S_4$ transition. The observed red-shift in the absorption maximum of T12-Ester (433 nm) compared to the one of T12 (416 nm) reflects a higher π -conjugation in the former owing to the carboxylphenyl groups that are surrounding the central core. For the three samples, the absorption band around 400-500

nm is assigned to the $S_0 \rightarrow S_1$ transition, while the band around 330 nm is assigned to the $S_0 \rightarrow S_2$ transition. It should be noted that when the molecular units of these materials are in solutions, such as in *N,N*-dimethylformamide and chloroform, the $S_0 \rightarrow S_1$ transition is symmetry forbidden (D_{3h}).^{28-29, 31, 36, 40-41} However, as we show here, when these molecules are the building blocks of their crystals, they are stacked through π - π interactions, losing the D_{3h} symmetry and thus, allowing the $S_0 \rightarrow S_1$ transition. Similar behaviour has been observed in platinum dihalide complexes containing 9-phenyl-9-arsafluorene (3-PtX_2 , X= Cl, Br, I).⁴² For these compounds, the HOMO-LUMO transitions in solution are forbidden, due to the symmetry that they present, although in solid state this transition becomes allowed. As mentioned above, the maximum of the absorption spectrum of T12-apo slightly differs from the ones of T12 and T12-Ester. The presence of benzoic acids in the molecular frame of T12-apo induces H-bond interactions between the T12-COOH units when making the crystals, in addition to the π - π ones. While these H-bonds are directional in making a HOF, they can extend or modify the crystalline structure of the material, leading to distortions in the symmetry of the building blocks, and thus, making allowed the $S_0 \rightarrow S_1$ transition. Therefore, based on the change in the absorption spectra of T12-apo, we believe that the benzoic acid moieties strongly affect the ordered structure of this material.

Because the absorption of solution and solid-state spectra are different, we also examined the emission and photodynamics properties of these materials under time-resolved fluorescence microscopy (with ~ 200 ps and 300 nm time and space resolution, respectively), in order to find a relationship between their crystals nature and photobehaviour for exploring their use in optoelectronic devices such as OLEDs.

3.2. Confocal Microscopy Fluorescence and Time-Resolved Studies

3.2.1. Crystals of 5,6,11,12,17,18-hexadehydrotribenzo[a,e,i]cyclododecene (T12)

We excited the crystals of T12 at 390 nm and recorded the fluorescence images, spectra and decays. Figure 2a shows the emission spectra recorded at different parts of a large ($> 20 \mu\text{m}$) crystal of T12. The inset of Figure 2a shows the fluorescence lifetime image (FLIM), while Figure 2b displays the emission spectrum along with a FLIM image of a smaller crystal ($< 0.5 \mu\text{m}$). The emission spectra recorded from five different positions of the large crystal are very similar exhibiting a well-resolved vibrational feature, with intensity maxima at: 479, 494, 504, 521, 531, 551, 563 nm. They are also similar to the one collected for the smaller crystal (Figure 2b). This recording indicates that the crystals size does not affect the luminescence properties of this material in solid state. This result is similar to all the examined T12 crystals, as shown for example in Figures S2a-S2c and S3a-S3c, where different crystals in size and shape exhibit similar emission spectra. The well-resolved vibrational emission band reflects a high rigidity and planarity of the molecular building blocks in this material, most probably due to strong π - π interactions.³⁶ This vibrational emission band also agrees with the IR spectrum of T12 (Figure 1a), which displays only few peaks, as the vibrations amplitude in this material is restricted by the rigidity and the strong π - π interactions.

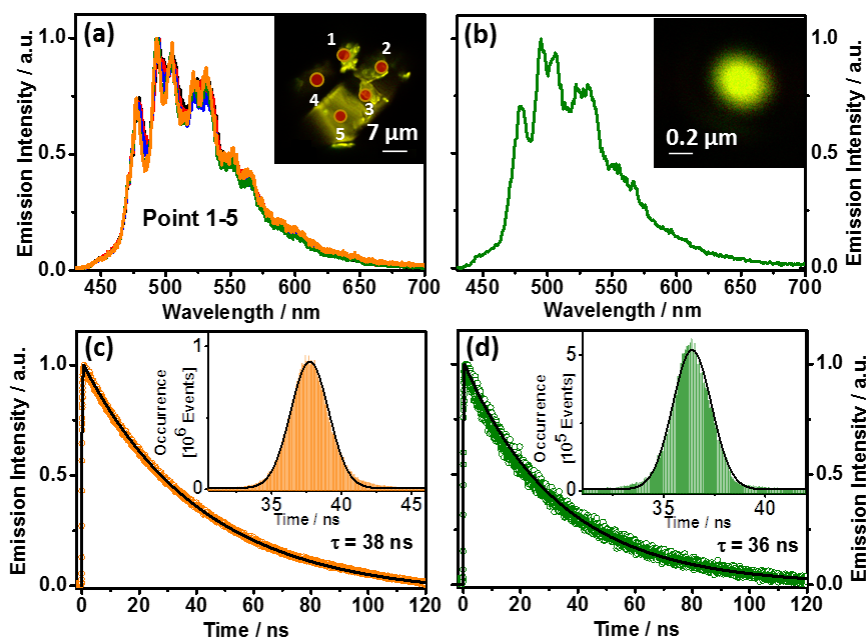


Figure 2. Emission spectra of (a) large and (b) small crystal of T12. The five emission spectra in (a) were recorded at different points as indicated in the FLIM image. Fluorescence emission decays of (c) large and (d) small crystals of T12. The excitation wavelength was 390 nm and the decays were recorded over the whole spectral range using a 430-nm long-pass filter. The solid lines are from the best-fit using a monoexponential function. The insets in (c) and (d) show the lifetime histograms.

Aiming a further understanding of the crystals photobehaviour, we performed time-resolved emission experiments on selected large and small crystals as well as averaged of over the whole crystals, Figures 2c-2d, respectively. The FLIM images of both, the large and small crystals, show a homogeneous distribution of the emission lifetimes. The decays collected on a large crystal give a very similar lifetime ~38 ns (Figure 2c). The analysis of the lifetimes distribution in the whole crystal presents a histogram (inserted in Figure 2c) centred at 37.7 ns, very similar to the one obtained from a single point (inset in Figure 2c). The lifetime distribution is symmetric with a full width at half maximum (FWHM) of 3.2 ns, reflecting a large homogeneity distribution of the

emitters. The mean emission lifetime of the small crystal has a value of 36 ns, which is similar to the value of 36.4 ns obtained from the lifetime distribution histogram of the full small crystal (Figure 2d). The FWHM is narrower (2.3 ns), which indicates less variation in the lifetimes with the position of observation in this crystal, and very similar emitters when compared to the situation of longer crystals. All the investigated T12 crystals are characterized by a long fluorescence lifetime (36-41 ns), Figures S2a'-2c' and S3a'-3c'.

To summarize this part, no difference between large and small crystal emission spectra were found; while, they exhibit a well resolved vibrational structure, contrary to the absorption spectrum. Moreover, the fluorescence lifetime distribution centred on 38 ns displays a value between 36 and 41 ns. In the following, we present and discuss the results of T12-Ester crystals, where the molecular unit has methoxycarbonylphenyl groups surrounding the DBA core that can make richer the photodynamics of T12-Ester in comparison to that of T12.

3.2.2. Crystals of 5,6,11,12,17,18-hexadehydro-2,3,8,9,14,15-hexakis(4-methoxycarbonylphenyl)tribenzo[a,e,i]cyclododecene (T12-Ester)

We have performed emission experiments on large ($> 40 \mu\text{m}$) and small ($\sim 0.5 \mu\text{m}$) crystals of T12-Ester (Figure 3a and 3b). The emission spectra of both, the large and small, are not very different, displaying a vibrational progression with maxima at 494 and 530, suggesting a priori no significant changes in the luminescence properties with the size of the crystals (more examples are given in Figure S4a-S4c and S5a-S5d). For the small ones, the spectrum also exhibits a shoulder located at 550 nm. Moreover, a close look at the peaks at 494 and 530 nm shows that the ratio ($I_{530}/I_{494}=\text{Ratio}$) of their intensities depends on the crystals size. While the ratio for the small crystals is 2.2, in the larger ones it is 3.0. This fact suggests the presence of a non-radiative process controlled by the size of the material. On the other hand, compared to the well-resolved emission

band of T12 crystals (Figure 2a and 2b), the one of T12-Ester is not so well resolved, which suggests that the outer benzoate branches provide more flexibility to the building blocks of this material, and thus affecting the vibrational energy redistribution in the excited crystals. This suggestion is supported by the IR spectra, in which T12-ester spectrum shows more peaks than the one of T12, reflecting the motion of the methoxycarbonylphenyl groups of T12-ester (Figure 1A). This kind of movement may affect the π - π interactions of the central core in the T12 crystals. Lifetime measurements will provide more information about this behaviour.

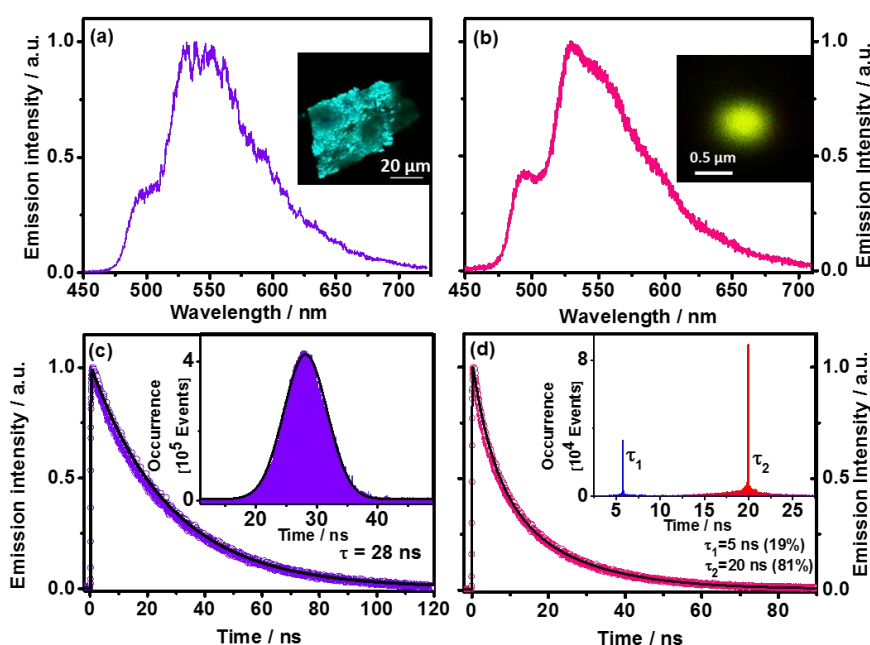


Figure 3. Emission spectra of (a) large and (b) small crystals of T12-Ester. The insets exhibit the FLIM images of the crystals. Fluorescence emission decays of (c) large and (d) small crystals of T12-Ester. The excitation wavelength was 390 nm and the decays were recorded over the whole spectral range using a 430-nm long-pass filter. The solid lines are from the best-fit using a mono- or multiexponential function. The insets show the lifetime distribution histograms.

Thus, we carried out picosecond time-resolved emission experiments on several large and small crystals (Figure 3c-3d). More examples are shown in supporting information (Figures S4a'-S4c' and S5a'-S5d'). Contrary to the lack of dependence of the observed emission lifetimes of T12 crystal on their sizes, for T12-Ester we observed a clear dependence of the photodynamical behaviour on the crystal size. While the emission decays of large crystals (5-20 μm) are monoexponential (giving a mean time constant of $\sim 25\text{-}28$ ns), the smaller ones (<1 μm) decay bi-exponentially with time constants of $\tau_1 \approx 4.5\text{-}5.5$ ns (pre-exponential factor, $a_1 \sim 20\text{-}45\%$) and $\tau_2 \approx 17\text{-}20$ ns (pre-exponential factor, $a_2 \sim 80\text{-}55\%$) (Figure 3c-3d, respectively).

The lifetime distribution histogram (Figure 3c) for the whole large crystals is centred on 28 ns, similar to the one obtained from the representative emission decays, with FWHM of 8.34 ns, reflecting a more heterogeneous distribution of the emitters when compared to the crystals of T12 (FWHM ≈ 3 ns, Figure 2c). Because the value of the lifetime is close to that of T12 crystals lacking the phenyl ester groups, we ascribe the 25-28 ns component to the fluorescence of the T12-Ester core, without much influence of the substituents on their decays.

For the smaller crystals, the lifetime distribution histogram shows two different emitters having lifetimes of 5 and 20 ns (Figure 3d). The origin of the longest component is similar to the one observed for larger crystals. We explain the 5-ns lifetime observed in the small crystals, in terms of the effect of conformation of the phenyl ester groups on their photobehaviour. This component is not observed in larger ones probably due to a closed packing of the constituent molecular units. Previously, we have reported on the occurrence of a photoinduced intramolecular charge transfers (ICT) reaction in T12-COOMe units in DMF solutions.³⁶ We have found a 4.5-ns component, which we assigned to the emission of a different species undergoing a charge transfer process

involving the external benzoate moieties. After photoexcitation, T12-COOMe in DMF solution experiences a fast electronic redistribution from the benzoate groups to the inner core, producing a charge transfer species emitting with a lifetime of 4.5 ns. This assignment was further supported by theoretical calculations.³⁶ Additionally, it is well known that porous materials (like MOFs and COFs) are prone to contain defects in their structure which may raise important changes in their luminescence properties.⁴³⁻⁴⁶ The presence of these defects can be relevant to the photocatalytic activity and lighting performance of the MOF based OLEDs.¹⁹ Here, we suggest that defects formed during the formation of small crystals, associated with the flexibility of the methoxycarbonylphenyl groups adopting different conformations, favouring the ICT process from the phenyl ester groups to the inner core. Thus, we ascribe the 5-ns component in the decays of the small crystals to the emission of species that have experienced an ICT reaction from the methoxycarbonylphenyl groups to the core of the unit.

To conclude this part, small differences in the emission spectra of large and small crystals were found. While large ones show a single emission lifetime of in the range 20-28 ns; for smaller ones, we recorded an additional short fluorescence lifetime (5 ns) assigned to the relaxation from CT excited state.

3.2.3. Crystals of 5,6,11,12,17,18-hexadehydro-2,3,8,9,14,15-hexakis(4-carboxyphenyl)tribenzo[a,e,i]cyclododecene (T12-apo)

T12-apo crystals are of particular interest because the molecular building blocks contain benzoic acid units as outer branches that can be involved in the crystallization through H-bond interactions, and thus inducing HOF formation.³⁷ Thus, in addition to the crystallization owing to π - π interactions between the central cores, as observed for T12 and T12-Ester, H-bond interactions may act as the driving force to stabilize the crystalline

structure of T12-apo, HOF (Scheme 1). One can expect that the emission properties of T12-apo based HOF may change reflecting the effect of the H-bonds between the units within the crystal. This behaviour has been reported recently for a carbonyl difluoroboron- β -diketone derivative, DBF-Ester [3-(4-(methoxycarbonyl)phenyl)-1-(4-methoxyphenyl)propane-1,3-dione (3)], which displays two different crystal packings and an amorphous form.⁴⁷ The fluorescence decays recorded for each system exhibit different lifetimes: 4.5 and 7.6 ns for crystalline structures, and 12.3 ns for the amorphous ones.⁴⁷

Thus, aiming a deeper knowledge on the photobehaviour of T12-apo HOF, we have recorded the emission spectra of several small ($\sim 0.3 - 1 \mu\text{m}$) and large ($>30 \mu\text{m}$) crystals (Figures 4 and 5 and Figure S6a-S6d). To begin with the smaller ones, we observed a clear dependence of the emission spectra on their shape and size. Some of them exhibit emission spectra similar to those observed for T12-Ester (Figure 3) with peaks having intensity maxima at 434 and 557 nm (Figures 4a-4b and S6a-S6b), while others emit at longer wavelengths, displaying the intensity maxima at 585 and 640 nm (Figures 4c-4d and Figures S6c-S6d). Because, the first type of crystals present photobehaviour comparable to the T12-Ester ones; thus, we suggest that their structure is governed by π - π interactions. The emission of the second family in the 500-550 nm region is weaker, contrary to the one in the reddest zone. These spectra are comparable to those of the building T12-COOH units when interacting with DMF molecules, where a strong H-bond interactions lead to a red shift in the emission spectrum as a result of the formation of T12-COO⁻ anion.³⁶ Therefore, the driving force for the formation of this type of crystals is based on H-bond interactions between the units owing to the presence of the benzoic acid branches. Thus, the red emission of the HOF crystals comes from species

having an experienced a photoinduced proton-transfer character between two H-bonded carboxylic groups.

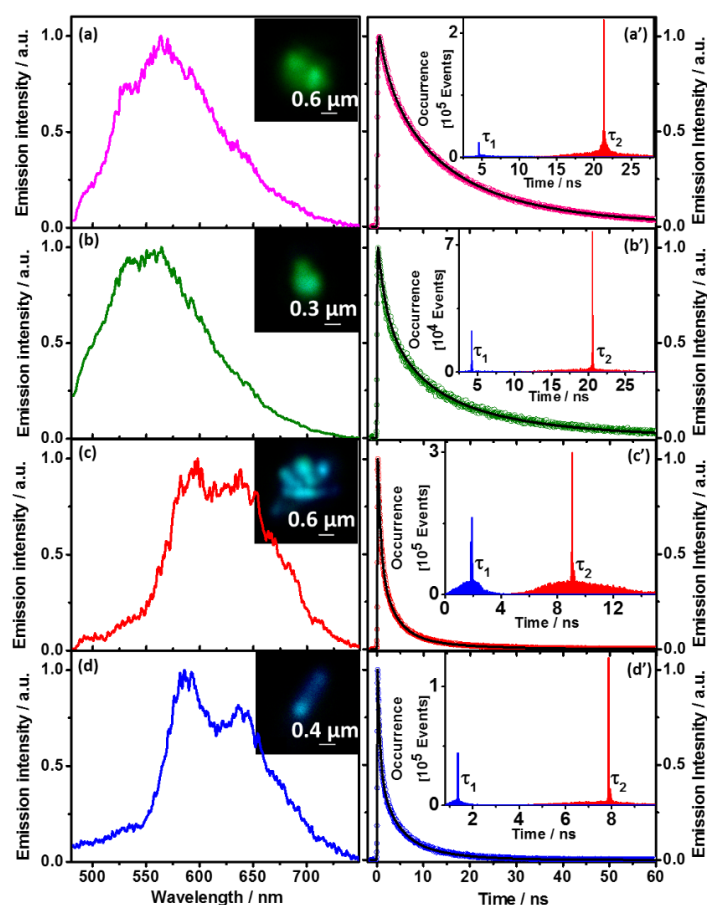


Figure 4. Emission (a-d) spectra and decays (a'-d') of small T12-apo crystals. The excitation wavelength was 390 nm and the decays were recorded over the whole spectral range using a 430-nm long-pass filter. The solid lines are from the best-fit using a multiexponential function. The insets in Figures (a-d) show the FLIM images of the samples, and those in Figures (a'-d') give the lifetime distribution histogram.

Crystal	τ_1 (ns) ± 0.2	a_1	τ_2 (ns) ± 0.3	a_2	τ_3 (ns) ± 0.3	a_3
1	4.5	38	-	-	21	62
2	4.1	48	-	-	20	52
3	1.5	25	8.8	75	-	-
4	1.4	23	8.5	77	-	-

Table 1. Values of time constants (τ_i) and normalized (to 100) pre-exponential factors (a_i) obtained from the fit of the emission decays of four samples of T12-apo shown in Figure 4. The decays were recorded over the whole spectral range using a 430-nm long-pass filter.

Figures 5 and S7 show the emission spectra of several larger crystals ($>30 \mu\text{m}$ in length) of T12-apo. Firstly, the spectra are remarkably different from those of smaller ones (Figures S4 and S6). Secondly, they are comparable to those described for T12-Ester and T12 (Figure 2 and 3). Thirdly, the spectra present well-resolved vibrational structure with maxima at 494, 528, 550 and 590 nm. This feature is not observed in the emission bands of the smaller crystals (Figure 4). Comparing the spectra to the one obtained for T12-ester large crystals, we observe a better vibrational structure. While the shape and position of the emission spectra of small T12-apo crystals show a great variation, these of the larger one does not show important variation changes.

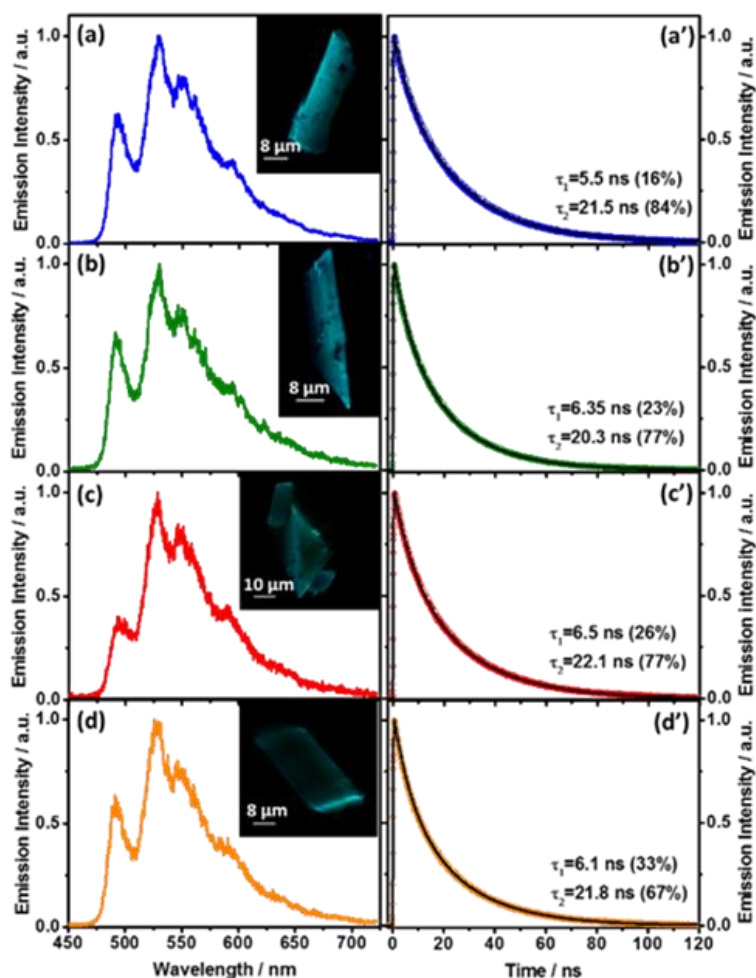


Figure 5. Emission (a-d) spectra and decays (a'-d') of the large T12-apo crystals. The excitation wavelength was 390 nm and the decays were recorded over the whole spectral range using a 430-nm long-pass filter. The solid lines are from the best-fit using a multiexponential function. The insets in Figures (a-d) show the images of the studied large crystals.

To explore the photodynamics of small and large crystals, we also investigated their emission decays (Figures 4, 5, S6 and S7). Remarkably, and in agreement with the steady-state behaviour, from the photodynamical behaviour (Figure 4a'-4d'), we can clearly distinguish two families of small crystals T12-apo. The first class shows longer decays, in similarity to the T12-Ester ones. The decays were fitted using a biexponential

function with time constants of 4.1-4.5 and 20-21 ns (Figure 4a and 4b and table 1). The lifetime distribution histogram for the whole crystal displays two different distributions centred on the same values as those obtained from the emission decays (Figure 4a and 4b). Both components of the histograms are homogeneously distributed along the crystal (Figure S6a-S6b gives more examples). In similarity with the explanation given for the T12-Ester decays, we assign the 20-ns component to the fluorescence of species not strongly affected by the H-bonds between the carboxylic groups, while the 4.1-4.5-ns one is due to emitters that have experienced an ICT reaction.

The second type of small crystals exhibits a biexponential behaviour with time constants of 1.4-1.5 and 8.5-8.8 ns (Figure 4c and 4d and Table 1). The lifetime distribution show two different populations of emitters (Figure 4c and 4d). More examples are given in ESI (Figure S6c-S6d). The short (1.5 ns) component is comparable to the one described for the charge transfer process (~1 ns) of the molecular building blocks of T12-apo in DMF (in addition to the 4.5 ns one).³⁶ We suggest that the H-bond interactions make this component faster in comparison with the one observed for T12-Ester (~5 ns). The value of the 8.8-ns component also becomes smaller when compared to the 20-ns one observed for the fluorescence of the first class of T12-apo crystals. The shortening also reflects the effect of the H-bonds in these structures that may lead to a proton-transfer reaction in the building blocks in agreement with the photobehaviour of T12-COOH molecules in DMF solution,³⁶ giving rise to the observed difference in the photobehaviour of the two families of small T12-apo crystals.

The photodynamics of the T12-apo large crystals of the HOF is similar to that of the first class of small T12-apo and that of the T12-Ester ones. It shows a biexponential behaviour with time constants of 4-6.5 and ~17-22 ns (Figures 5 and S7). The longest component is comparable to that observed in T12-ester (28 ns), and thus is assigned to

species not affected by the presence of the H-bonds in the HOF. However, we attribute the shortest component to species undergoing an ICT reaction. In contrast to the photobehaviour of the large T12-Ester crystals, for small and large ones of T12-apo we got the contribution of the component assigned to ICT process in their emission decays. This difference might be explained in terms of the presence of H-bonds in T12-apo, that on one hand, stabilize the conformation of the carboxylic groups and on the other, modify the electronic charge distribution within the building units of the HOF.

As commented above, the intensity of some peaks changes with the nature of the crystals, hence, we recorded the emission decays of in selected parts of the emission spectrum: 480-520 nm region and from 530 nm to the end of the spectrum, (Figure S7). For the same crystals, the obtained result recording at both regions are very similar 4.6-5 ns (28-30%) and 19-20 ns (70-72%). Therefore, the emitters display overlapping and similar emission bands, generating the observed spectrum. From the spectroscopic and photodynamical behaviour of the large T12-apo crystals, we suggest that in addition to the role played by the H-bonds between the building blocks of this HOF, the π - π stacking interactions contribute relevantly in the process of crystallization.

To summarize this part, we conclude that two different crystals can be formed, depending on the predominant type of interactions between the T12-apo units involving π - π stacking interactions or intermolecular H-bonds. The first family displays a photobehaviour similar to that of T12 and T12-Ester, and thus π - π interactions play the main role in their structures. The second one, the H-bonds dictate their crystallinity and shape. The last ones exhibit a red-shifted emission spectrum and a shorter lifetime (9-11 ns), assigned to species having experience a proton-transfer reaction within the HOF. However, without the contribution of the H-bonds between the units, the crystalline large structure cannot be formed.

3.2.4. Emission Anisotropy of Large T12-Ester and T12-apo Crystals

The action of different driving forces in the crystallization process of T12-apo to build the corresponding HOF suggests also variation in the anisotropic properties of the crystals emission. Thus, we performed anisotropy measurements at two different crystal orientations. Firstly, we recorded the FLIM image of a crystal, and then, we 90° rotate the sample holder with respect to the previous position, and again recorded the FLIM. For simplicity, we label the first and second position as 1 and 2, respectively. Using the static anisotropy, we build the anisotropy histogram, as described in the experimental part. Figure 6 shows a representative image of two large crystal (>20 μm) and representative histograms of the steady-state anisotropy values distribution at two crystal orientations (1 and 2 with respect to the observation plane, respectively). Additional examples are given in Figure S8. Moreover, the studies crystal in Figure 6 (a) and (a') has a smaller crystal ($\sim 5 \times 5 \mu\text{m}^2$) attached to its surface.

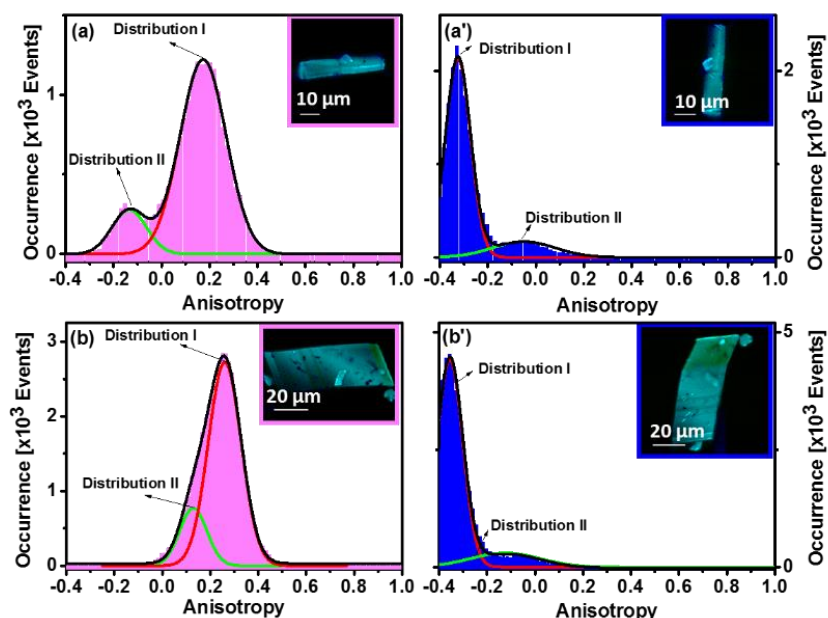


Figure 6. Histograms of the emission anisotropy of T12-apo crystals observed at position 1 for (a) and (b) and position 2 for (a') and (b'). The solid lines represent Gaussian fits to the anisotropy histograms. The insets show images of the crystals.

The histograms show a clear evidence for the presence of two different crystal types that differ in their emission anisotropy behaviour. The histograms for all the crystals at both orientations are fitted by two Gaussians. The first distribution (distribution I) that has the larger contribution, demonstrates strong dependence of the anisotropy value on the crystal orientation (Table S1, Figures 6 and S8). For the 1 crystal orientation, the anisotropy is centred on positive values between 0.19 and 0.48 that shifts to strongly negative values for the 2 orientations (the crystal rotated 90° with respect to the 1 orientation) between -0.19 and -0.36 (Table S1). The strong dependence of the anisotropy value for this type of crystals suggests preferential orientation of the molecular units inside the crystal structure. The second distribution (distribution II), which is broader and has a smaller contribution to the overall histogram, has the maximum of the anisotropy value close to zero (between -0.24 and 0.24), and shows little dependence on the crystal orientation. Additional analysis of discrete regions corresponding to the interrogated small and the large crystals shown in Figure 6 allows for the correct assignment of the two Gaussian distributions (Figure S9). The Gaussian distribution centred on -0.18 and -0.13 with 18 and 17 % relative contribution, respectively, in both histograms arises from the anisotropy behaviour of the smaller crystal, while those centred on 0.10 and -0.31 (1 and 2, respectively) corresponds to the large crystal. Similar conclusion can be drawn for the rest of the studied HOF crystals, where distribution II arises predominantly from smaller crystals attached to the surface of the larger crystals, Figure S8. Thus, the lack of dependence of the anisotropy value on the orientation (distribution II) for the small ones suggests that there is no preferential orientation of the molecular units that form the crystal, and thus its behaviour is almost isotropic. It should be noted that certain degree of crystallinity is achieved in these small crystals that gives rise to the anisotropy values

that are different from the pure isotropic behaviour. This crystallinity is most probably a result of H-bonding interactions between the elementary units, as suggested also from the photodynamical behaviour of the two families of small T12-apo crystals. The anisotropy experiments using large crystals of T12-Ester, and lacking H-bond interactions (Figure S10), agree with the above discussion. The overall histogram is centred on 0.05 and 0.04. Hence, there is no preferential orientation of the molecular units of T12-Ester suggesting that this material is mostly an amorphous solid.

Thus, to conclude this part, the crystallization of T12-apo is dominated by π - π stacking interactions, although stabilized by H-bonds; the molecular units have preferential orientation which results in the observed anisotropic behaviour of the HOF. Similar anisotropic behaviour has been reported for crystals formed by hexakis(4-carboxy-phenyl)-hexaazatriphenylene, where the fluorescence microscopy study at single crystal level reveals an ordered crystalline structure with a preferential orientation of the molecular units.³⁵

3.2.5. CIE coordinates of T12-apo

The characterization of new smart materials is essential in order to fabricate new efficient devices, free from rare-earth elements, because of the limited amounts and high price of these compounds, moreover most of the commercial WLEDs are fabricated using YAG:Ce³⁺ (CIE coordinates= 0.41, 0.56) acts as phosphor.^{19, 48-55} T12-apo has a CIE coordinates of (0.42, 0.55) (Figure S11), which are similar to those of YAG:Ce³⁺. T12-apo could be a good candidate to use in the fabrication of WLEDs, free of any metal. Moreover, T12-apo in solid state displays a fluorescence quantum yield of 25%, higher than that of T12.^{31, 37} This relatively high value and its CIE coordinates suggest to use it as a material to fabricate WLEDs. The increment in the emission quantum yield and the discovery of two kinds of T12-apo crystals of different emission spectra and lifetimes

(Figure 4 and 5) suggest further improvements in the crystallization process of the related HOF, in order to get a good candidate to fabricate an efficient WLEDs. One can coat a blue-LED with this HOF and get a LED with tunable emission wavelength, as it has been reported for other materials.^{51, 54-55}

4. Conclusions

In this work, we have explored on the spectroscopic and photodynamics properties of a series of DBA derivative based materials: T12, T12-Ester and T12-apo. Contrary to the observed for the absorption spectra of the molecular building blocks in DMF solutions, where the $S_0 \rightarrow S_1$ transition is forbidden, in the solid state this transition becomes allowed, due to a change in the molecular symmetry when the networks are formed. Single crystal confocal fluorescence microscopy experiments of T12 show that the emission spectra and lifetimes (~ 38 ns) for both small and large crystals are similar. However, large and small crystals of T12-Ester exhibit a different photodynamical behaviour. While the emission of the large ones decays monoexponentially (28 ns), the small ones show a biexponential behaviour with time constants of ~ 5 and ~ 20 ns. The shortest component reflects the emission of the species that have undergone an ICT process. Remarkably, T12-apo crystals present different emission spectra and decays. Our analysis suggests that crystals exhibiting emission spectra and decays like T12 and T12-Ester, are governed mainly by π - π interactions, while others have different behaviour where the H-bonds between the building blocks play a role in the crystallization and photochemistry. The HOF crystals exhibits (in addition to the S_1 and S_{CT} emission) emission from species that exhibit a proton-transfer character. The anisotropy experiments on T12-apo suggest that the main driving force for the crystals formation are the π - π stacking interactions. However, these interactions directed by H-bonds are making preferential orientation of the building units. We suggest that T12-apo could be a potential

candidate for an OLED of wide emission spectrum, when coating a blue-LED. The results of this work provide new insight for further improvement of this HOF material aiming its use in efficient and versatile lighting devices.

Acknowledgments

This work was supported by the MINECO through projects: MAT2014-57646-P and MAT2017-86532-R. E. G. thanks the MINECO for the Ph.D. fellowship. I.H. thanks a Grant-in-Aid for Scientific Research (C) (JPT15K04591) from MEXT Japan. We thank Prof. Shu Seki at Kyoto University for SEM measurements.

Supporting Information

The supporting information gives complete infrared spectra of T12, T12-ester and T12-apo; and SEM images of T12-apo. For all the materials, the supporting information also gives more emission spectra and decays of different crystals. It also shows more examples of the emission anisotropy of T12-Ester and T12-apo. Finally, it provides the figure for the CIE coordinates of T12-apo.

References

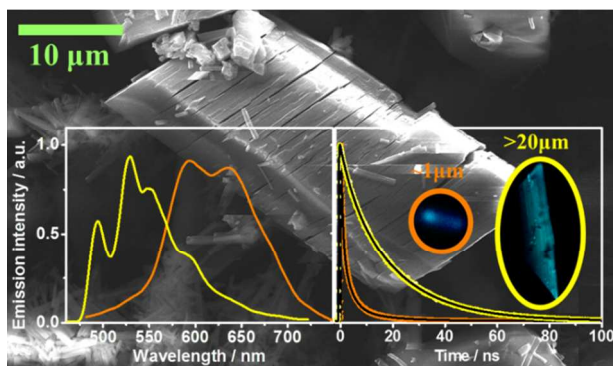
1. Slater, A. G.; Cooper, A. I., Function-led design of new porous materials. *Science* **2015**, *348* (6238).
2. Mintova, S.; Jaber, M.; Valtchev, V., Nanosized microporous crystals: emerging applications. *Chem. Soc. Rev.* **2015**, *44* (20), 7207-7233.
3. Alarcos, N.; Cohen, B.; Ziótek, M.; Douhal, A., Photochemistry and Photophysics in Silica-Based Materials: Ultrafast and Single Molecule Spectroscopy Observation. *Chem. Rev.* **2017**, *117* (22), 13639-13720.
4. Cui, Y.; Yue, Y.; Qian, G.; Chen, B., Luminescent Functional Metal–Organic Frameworks. *Chem. Rev.* **2012**, *112* (2), 1126-1162.
5. Feng, X.; Ding, X.; Jiang, D., Covalent organic frameworks. *Chem. Soc. Rev.* **2012**, *41* (18), 6010-6022.
6. Côté, A. P.; Benin, A. I.; Ockwig, N. W.; Keeffe, M.; Matzger, A. J.; Yaghi, O. M., Porous, Crystalline, Covalent Organic Frameworks. *Science* **2005**, *310* (5751), 1166.
7. Waller, P. J.; Lyle, S. J.; Osborn Popp, T. M.; Diercks, C. S.; Reimer, J. A.; Yaghi, O. M., Chemical Conversion of Linkages in Covalent Organic Frameworks. *J. Am. Chem. Soc.* **2016**, *138* (48), 15519-15522.
8. Ma, L.; Wang, S.; Feng, X.; Wang, B., Recent advances of covalent organic frameworks in electronic and optical applications. *Chin. Chem. Lett.* **2016**, *27* (8), 1383-1394.
9. Mandal, A. K.; Mahmood, J.; Baek, J.-B., Two-Dimensional Covalent Organic Frameworks for Optoelectronics and Energy Storage. *ChemNanoMat* **2017**, *3* (6), 373-391.
10. Wu, M.-X.; Yang, Y.-W., Applications of covalent organic frameworks (COFs): From gas storage and separation to drug delivery. *Chin. Chem. Lett.* **2017**, *28* (6), 1135-1143.
11. Rogge, S. M. J.; Bavykina, A.; Hajek, J.; Garcia, H.; Olivos-Suarez, A. I.; Sepulveda-Escribano, A.; Vimont, A.; Clet, G.; Bazin, P.; Kapteijn, F.; Daturi, M.; Ramos-Fernandez, E. V.; Llabres i Xamena, F. X.; Van Speybroeck, V.; Gascon, J., Metal-organic and covalent organic frameworks as single-site catalysts. *Chem. Soc. Rev.* **2017**, *46* (11), 3134-3184.
12. Xie, Y.-F.; Ding, S.-Y.; Liu, J.-M.; Wang, W.; Zheng, Q.-Y., Triazatruxene based covalent organic framework and its quick-response fluorescence-on nature towards electron rich arenes. *J. Mater. Chem. C* **2015**, *3* (39), 10066-10069.
13. Hu, Z.; Deibert, B. J.; Li, J., Luminescent metal-organic frameworks for chemical sensing and explosive detection. *Chem. Soc. Rev.* **2014**, *43* (16), 5815-5840.
14. Huang, Y.-B.; Liang, J.; Wang, X.-S.; Cao, R., Multifunctional metal-organic framework catalysts: synergistic catalysis and tandem reactions. *Chem. Soc. Rev.* **2017**, *46* (1), 126-157.
15. Chughtai, A. H.; Ahmad, N.; Younus, H. A.; Laypkov, A.; Verpoort, F., Metal-organic frameworks: versatile heterogeneous catalysts for efficient catalytic organic transformations. *Chem. Soc. Rev.* **2015**, *44* (19), 6804-6849.
16. Silva, P.; Vilela, S. M. F.; Tome, J. P. C.; Almeida Paz, F. A., Multifunctional metal-organic frameworks: from academia to industrial applications. *Chem. Soc. Rev.* **2015**, *44* (19), 6774-6803.
17. Stassen, I.; Burtch, N.; Talin, A.; Falcaro, P.; Allendorf, M.; Ameloot, R., An updated roadmap for the integration of metal-organic frameworks with electronic devices and chemical sensors. *Chem. Soc. Rev.* **2017**, *46* (11), 3185-3241.
18. Crowe, J. W.; Baldwin, L. A.; McGrier, P. L., Luminescent Covalent Organic Frameworks Containing a Homogeneous and Heterogeneous Distribution of Dehydrobenzoannulene Vertex Units. *J. Am. Chem. Soc.* **2016**, *138* (32), 10120-10123.
19. Gutiérrez, M.; Martin, C.; Kennes, K.; Hofkens, J.; Van der Auweraer, M.; Sánchez, F.; Douhal, A., New OLEDs Based on Zirconium Metal-Organic Framework. *Adv. Opt. Mater.* **2018**, *6* (6).
20. Lustig, W. P.; Mukherjee, S.; Rudd, N. D.; Desai, A. V.; Li, J.; Ghosh, S. K., Metal-organic frameworks: functional luminescent and photonic materials for sensing applications. *Chem. Soc. Rev.* **2017**, *46* (11), 3242-3285.

21. Han, Y.-F.; Yuan, Y.-X.; Wang, H.-B., Porous Hydrogen-Bonded Organic Frameworks. *Molecules* **2017**, *22* (2), 266.
22. Yang, W.; Yang, F.; Hu, T.-L.; King, S. C.; Wang, H.; Wu, H.; Zhou, W.; Li, J.-R.; Arman, H. D.; Chen, B., Microporous Diaminotriazine-Decorated Porphyrin-Based Hydrogen-Bonded Organic Framework: Permanent Porosity and Proton Conduction. *Cryst. Growth Des.* **2016**, *16* (10), 5831-5835.
23. Hu, F.; Liu, C.; Wu, M.; Pang, J.; Jiang, F.; Yuan, D.; Hong, M., An Ultrastable and Easily Regenerated Hydrogen-Bonded Organic Molecular Framework with Permanent Porosity. *Angew. Chem. Int. Ed.* **2017**, *56* (8), 2101-2104.
24. Karmakar, A.; Illathvalappil, R.; Anothumakkool, B.; Sen, A.; Samanta, P.; Desai, A. V.; Kurungot, S.; Ghosh, S. K., Hydrogen-Bonded Organic Frameworks (HOFs): A New Class of Porous Crystalline Proton-Conducting Materials. *Angew. Chem. Int. Ed.* **2016**, *55* (36), 10667-10671.
25. Sun, Z.; Li, Y.; Chen, L.; Jing, X.; Xie, Z., Fluorescent Hydrogen-Bonded Organic Framework for Sensing of Aromatic Compounds. *Cryst. Growth Des.* **2015**, *15* (2), 542-545.
26. Wang, H.; Li, B.; Wu, H.; Hu, T.-L.; Yao, Z.; Zhou, W.; Xiang, S.; Chen, B., A Flexible Microporous Hydrogen-Bonded Organic Framework for Gas Sorption and Separation. *J. Am. Chem. Soc.* **2015**, *137* (31), 9963-9970.
27. Li, P.; He, Y.; Zhao, Y.; Weng, L.; Wang, H.; Krishna, R.; Wu, H.; Zhou, W.; O'Keeffe, M.; Han, Y.; Chen, B., A Rod-Packing Microporous Hydrogen-Bonded Organic Framework for Highly Selective Separation of C₂H₂/CO₂ at Room Temperature. *Angew. Chem. Int. Ed.* **2015**, *54* (2), 574-577.
28. Tahara, K.; Yamamoto, Y.; Gross, D. E.; Kozuma, H.; Arikuma, Y.; Ohta, K.; Koizumi, Y.; Gao, Y.; Shimizu, Y.; Seki, S.; Kamada, K.; Moore, J. S.; Tobe, Y., Syntheses and Properties of Graphyne Fragments: Trigonally Expanded Dehydrobenzo[12]annulenes. *Chem. Eur. J.* **2013**, *19* (34), 11251-11260.
29. Yoshimura, T.; Inaba, A.; Sonoda, M.; Tahara, K.; Tobe, Y.; Williams, R. V., Synthesis and Properties of Trefoil-Shaped Tris(hexadehydrotribenzo[12]annulene) and Tris(tetradehydrotribenzo[12]annulene). *Org. Lett.* **2006**, *8* (14), 2933-2936.
30. Johnson, C. A.; Lu, Y.; Haley, M. M., Carbon Networks Based on Benzocyclynes. 6. Synthesis of Graphyne Substructures via Directed Alkyne Metathesis. *Org. Lett.* **2007**, *9* (19), 3725-3728.
31. Hisaki, I.; Sakamoto, Y.; Shigemitsu, H.; Tohnai, N.; Miyata, M.; Seki, S.; Saeki, A.; Tagawa, S., Superstructure-Dependent Optical and Electrical Properties of an Unusual Face-to-Face, π -Stacked, One-Dimensional Assembly of Dehydrobenzo[12]annulene in the Crystalline State. *Chem. Eur. J.* **2008**, *14* (14), 4178-4187.
32. Zentner, C. A.; Lai, H. W. H.; Greenfield, J. T.; Wisconsin, R. A.; Zeller, M.; Campana, C. F.; Talu, O.; FitzGerald, S. A.; Rowsell, J. L. C., High surface area and Z[prime or minute] in a thermally stable 8-fold polycatenated hydrogen-bonded framework. *Chem. Commun.* **2015**, *51* (58), 11642-11645.
33. Nandi, S.; Chakraborty, D.; Vaidhyanathan, R., A permanently porous single molecule H-bonded organic framework for selective CO₂ capture. *Chem. Commun.* **2016**, *52* (45), 7249-7252.
34. Yu, T.; Ou, D.; Yang, Z.; Huang, Q.; Mao, Z.; Chen, J.; Zhang, Y.; Liu, S.; Xu, J.; Bryce, M. R.; Chi, Z., The HOF structures of nitrotetraphenylethene derivatives provide new insights into the nature of AIE and a way to design mechanoluminescent materials. *Chem. Sci.* **2017**, *8* (2), 1163-1168.
35. Hisaki, I.; Ikenaka, N.; Gomez, E.; Cohen, B.; Tohnai, N.; Douhal, A., Hexaazatriphenylene - Based Hydrogen - Bonded Organic Framework with Permanent Porosity and Single - Crystallinity. *Chem. Eur. J.* **2017**, *23* (48), 11611-11619.
36. Gomez, E.; Gutierrez, M.; Moreno, M.; Hisaki, I.; Nakagawa, S.; Douhal, A., Spectroscopy and dynamics of dehydrobenzo[12]annulene derivatives possessing peripheral carboxyphenyl groups: theory and experiment. *Phys. Chem. Chem. Phys.* **2018**, *20* (11), 7415-7427.

37. Hisaki, I.; Nakagawa, S.; Ikenaka, N.; Imamura, Y.; Katouda, M.; Tashiro, M.; Tsuchida, H.; Ogoshi, T.; Sato, H.; Tohnai, N.; Miyata, M., A Series of Layered Assemblies of Hydrogen-Bonded, Hexagonal Networks of C₃-Symmetric π -Conjugated Molecules: A Potential Motif of Porous Organic Materials. *J. Am. Chem. Soc.* **2016**, *138* (20), 6617-6628.
38. Huynh, C.; Linstrumelle, G., A short route to dehydro [12] annulenes. *Tetrahedron* **1988**, *44* (20), 6337-6344.
39. Schaffer, J.; Volkmer, A.; Eggeling, C.; Subramaniam, V.; Striker, G.; Seidel, C. A. M., Identification of Single Molecules in Aqueous Solution by Time-Resolved Fluorescence Anisotropy. *J. Phys. Chem. A* **1999**, *103* (3), 331-336.
40. Wirz, J., *In Excited States in Organic Chemistry and Biology*; 1977; p 283-294.
41. Nishide, H.; Takahashi, M.; Takashima, J.; Pu, Y.-J.; Tsuchida, E., Acyclic and Cyclic Di- and Tri(4-oxophenyl-1,2-phenyleneethynylene)s: Their Synthesis and Ferromagnetic Spin Interaction. *J. Org. Chem.* **1999**, *64* (20), 7375-7380.
42. Imoto, H.; Tanaka, S.; Kato, T.; Watase, S.; Matsukawa, K.; Yumura, T.; Naka, K., Highly Efficient Solid-State Phosphorescence of Platinum Dihalide Complexes with 9-Phenyl-9-arsafluorene Ligands. *Organometallics* **2016**, *35* (3), 364-369.
43. Heine, J.; Muller-Buschbaum, K., Engineering metal-based luminescence in coordination polymers and metal-organic frameworks. *Chem. Soc. Rev.* **2013**, *42* (24), 9232-9242.
44. Whittington, C. L.; Wojtas, L.; Gao, W.-Y.; Ma, S.; Larsen, R. W., A new photoactive Ru(ii)tris(2,2[prime or minute]-bipyridine) templated Zn(ii) benzene-1,4-dicarboxylate metal organic framework: structure and photophysical properties. *Dalton Trans.* **2015**, *44* (12), 5331-5337.
45. Fang, Z.; Bueken, B.; De Vos, D. E.; Fischer, R. A., Defect-Engineered Metal–Organic Frameworks. *Angew. Chem. Int. Ed.* **2015**, *54* (25), 7234-7254.
46. Reshchikov, M. A.; Morkoç, H., Luminescence properties of defects in GaN. *J. Appl. Phys.* **2005**, *97* (6), 5-19.
47. Louis, M.; Brosseau, A.; Guillot, R.; Ito, F.; Allain, C.; Métivier, R., Polymorphism, Mechanofluorochromism, and Photophysical Characterization of a Carbonyl Substituted Difluoroboron- β -Diketone Derivative. *J. Phys. Chem. C* **2017**, *121* (29), 15897-15907.
48. Wang, M.-S.; Guo, S.-P.; Li, Y.; Cai, L.-Z.; Zou, J.-P.; Xu, G.; Zhou, W.-W.; Zheng, F.-K.; Guo, G.-C., A Direct White-Light-Emitting Metal–Organic Framework with Tunable Yellow-to-White Photoluminescence by Variation of Excitation Light. *J. Am. Chem. Soc.* **2009**, *131* (38), 13572-13573.
49. Luo, F.; Wang, M.-S.; Luo, M.-B.; Sun, G.-M.; Song, Y.-M.; Li, P.-X.; Guo, G.-C., Functionalizing the pore wall of chiral porous metal-organic frameworks by distinct -H, -OH, -NH₂, -NO₂, -COOH shutters showing selective adsorption of CO₂, tunable photoluminescence, and direct white-light emission. *Chem. Commun.* **2012**, *48* (48), 5989-5991.
50. Sun, C.-Y.; Wang, X.-L.; Zhang, X.; Qin, C.; Li, P.; Su, Z.-M.; Zhu, D.-X.; Shan, G.-G.; Shao, K.-Z.; Wu, H.; Li, J., Efficient and tunable white-light emission of metal–organic frameworks by iridium-complex encapsulation. **2013**, *4*, 2717.
51. Gong, Q.; Hu, Z.; Deibert, B. J.; Emge, T. J.; Teat, S. J.; Banerjee, D.; Mussman, B.; Rudd, N. D.; Li, J., Solution Processable MOF Yellow Phosphor with Exceptionally High Quantum Efficiency. *J. Am. Chem. Soc.* **2014**, *136* (48), 16724-16727.
52. Deibert, B. J.; Velasco, E.; Liu, W.; Teat, S. J.; Lustig, W. P.; Li, J., High-Performance Blue-Excitable Yellow Phosphor Obtained from an Activated Solvochromic Bismuth-Fluorophore Metal–Organic Framework. *Cryst. Growth Des.* **2016**, *16* (8), 4178-4182.
53. Yu, X.-M.; Zhou, G.-J.; Lam, C.-S.; Wong, W.-Y.; Zhu, X.-L.; Sun, J.-X.; Wong, M.; Kwok, H.-S., A yellow-emitting iridium complex for use in phosphorescent multiple-emissive-layer white organic light-emitting diodes with high color quality and efficiency. *J. Organomet. Chem.* **2008**, *693* (8), 1518-1527.

54. Gutierrez, M.; Sanchez, F.; Douhal, A., Efficient multicolor and white light emission from Zr-based MOF composites: spectral and dynamic properties. *J. Mater. Chem. C* **2015**, *3* (43), 11300-11310.
55. Hu, Z.; Huang, G.; Lustig, W. P.; Wang, F.; Wang, H.; Teat, S. J.; Banerjee, D.; Zhang, D.; Li, J., Achieving exceptionally high luminescence quantum efficiency by immobilizing an AIE molecular chromophore into a metal-organic framework. *Chem. Commun.* **2015**, *51* (15), 3045-3048.

Table of Contents



T12-apo based HOF shows a dependence of its emission spectra and lifetimes on the crystal size, where π - π interactions and H-bonds network are paramount to the crystal nature and photobehaviour.